


## Phase estimation via a number-conserving operation inside a SU(1,1) interferometer

Qingqian Kang <sup>1,2</sup>, Zekun Zhao,<sup>1</sup> Teng Zhao,<sup>1</sup> Cunjin Liu,<sup>1</sup> and Liyun Hu<sup>1,3,\*</sup>

<sup>1</sup>Center for Quantum Science and Technology, Jiangxi Normal University, Nanchang 330022, China

<sup>2</sup>Department of Physics, College of Science and Technology, Jiangxi Normal University, Nanchang 330022, China

<sup>3</sup>Institute for Military-Civilian Integration of Jiangxi Province, Nanchang 330200, China



(Received 9 April 2024; revised 18 July 2024; accepted 7 August 2024; published 23 August 2024)

Utilizing nonlinear elements, SU(1,1) interferometers demonstrate superior phase sensitivity compared to passive interferometers. However, the precision is significantly impacted by photon losses, particularly internal losses. We propose a theoretical scheme to improve the precision of phase measurement using homodyne detection by implementing a number-conserving operation (NCO), i.e.,  $aa^\dagger$  and  $a^\dagger a$ , inside the SU(1,1) interferometer, with the coherent state and the vacuum state as the input states. We analyze the effects of the NCO on the phase sensitivity, the quantum Fisher information (QFI), and the quantum Cramér-Rao bound under both ideal and photon-loss scenarios. Our findings reveal that the internal non-Gaussian operations can enhance the phase sensitivity and the QFI and effectively improve the robustness of the SU(1,1) interferometer against internal photon losses. Notably, the  $a^\dagger a$  scheme exhibits superior improvement in both the ideal and photon-loss cases in terms of phase sensitivity. Moreover, in the ideal case, the  $aa^\dagger$  scheme slightly outperforms the  $a^\dagger a$  scheme in terms of the QFI. However, in the presence of high photon losses, the  $a^\dagger a$  scheme demonstrates a greater advantage.

DOI: [10.1103/PhysRevA.110.022432](https://doi.org/10.1103/PhysRevA.110.022432)

### I. INTRODUCTION

Optical interference measurement plays a crucial role in many scientific and technological applications such as quantum metrology for precise measurements, imaging for capturing detailed visual information, sensing for detecting and measuring physical quantities, and information processing for manipulating and transmitting data [1–9]. Consequently, there has been extensive research and significant advancements in the field of optical interference measurement. To satisfy the need for high precision, a variety of optical interferometers have been proposed and developed. One of the most practical interferometers is the Mach-Zehnder interferometer (MZI), whose phase sensitivity is limited by the standard quantum-noise limit (SQL)  $\Delta\phi = 1/\sqrt{N}$  ( $N$  is the average number of photons within the interferometer), together with solely classical resources as the input of the MZI [10]. In recent decades, various schemes have been proposed to improve the phase sensitivity of the traditional MZI [11,12]. It has been demonstrated that using quantum states as the input states to make the traditional MZI beat the SQL. For example, NOON states [13,14], twin Fock states [15], and the squeezed state [16,17] can achieve or even exceed the Heisenberg limit (HL)  $\Delta\phi = 1/N$  [18,19].

Another possibility to realize quantum-enhanced phase sensitivity is the SU(1,1) interferometer [20,21], which replaced traditional linear beam splitters (BSs) with optical parametric amplifiers (OPAs). It splits and mixes beams using nonlinear transformations, which was first proposed by

Yurke *et al.* [22]. In the SU(1,1) interferometer comprising two OPAs, the first OPA serves the dual purpose of acquiring entangled resources and suppressing amplified noise. Meanwhile, the subsequent use of the second OPA can lead to signal enhancement, offering a viable pathway for achieving higher precision in phase estimation. By utilizing entangled photon states, the SU(1,1) interferometer can surpass the SQL, enabling higher precision. This technique revolutionized phase estimation, becoming a vital tool in quantum precision measurements. As a result, there has been significant interest in studying the SU(1,1) interferometer [23–26]. For instance, Hudelist *et al.* demonstrated that the gain effect of the OPA results in the SU(1,1) interferometer exhibiting higher sensitivity compared to traditional linear interferometers [27]. In 2011, Jing *et al.* [28] successfully implemented this interferometer experimentally. In this nonlinear interferometer, the maximum output intensity can be much higher than that of a linear interferometer due to the OPA. Apart from the standard form, various configurations of the SU(1,1) interferometer have also been proposed [24,29–37].

As previously mentioned, although the SU(1,1) interferometer is highly valuable for precision measurement [38,39], the precision is still affected by dissipation, particularly photon losses inside the interferometer [40,41]. Consequently, to further enhance precision, non-Gaussian operations should serve as an effective approach to mitigate internal dissipation. Most theoretical [42–45] and experimental [46–48] studies have fortunately indicated that non-Gaussian operations, such as photon subtraction (PS), photon addition (PA), photon catalysis (PC), and quantum scissors and their coherent superposition, effectively enhance the nonclassicality and entanglement degrees of quantum states, thereby enhancing

\*Contact author: hlyun@jxnu.edu.cn

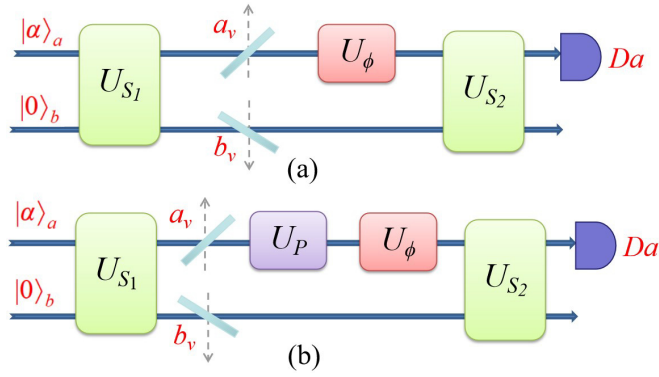


FIG. 1. Schematic diagram of the SU(1,1) interferometer. (a) The standard SU(1,1) interferometer and (b) the SU(1,1) interferometer with the NCO. The two input ports are a coherent state  $|\alpha\rangle_a$  and a vacuum state  $|0\rangle_b$ .  $a_v$  and  $b_v$  are vacuum modes.  $U_{S_1}$  and  $U_{S_2}$  are the optical parametric amplifiers, and  $U_\phi$  is the phase shifter.  $U_P$  is the NCO operator, and  $D_a$  is the homodyne detector.

their potential in quantum information processing [49,50]. Experimental studies have illustrated the conditional generation of superpositions of distinct quantum operations through single-photon interference, providing a practical approach for preparing non-Gaussian operations [51]. This advancement has unveiled new possibilities in quantum state manipulation and implications for various quantum technologies. In Ref. [52], Zhang *et al.* proposed a number-conserving operation (NCO) on the inputs of the MZI for improving the resolution and precision of phase measurement with parity detection. They showed that the phase sensitivity can be better than that of both the photon-subtraction operation and photon-addition operation in the presence of photon losses. Different from Ref. [52], Xu *et al.* examined the phase sensitivity with internal photon losses in SU(1,1) interferometers, rather than in the MZI, an SU(2) interferometer. They found that performing photon-addition operations internally provides superior results compared to those at the input [53]. Thus, a question arises naturally: can the NCO be operated inside the SU(1,1) interferometer (i.e., the non-Gaussian operation on the output states after the first OPA) to mitigate the impact of internal photon losses?

Therefore, in this paper, we concentrate on employing the NCO scheme inside the SU(1,1) interferometer to enhance the measurement accuracy and then analyze the improvement effect of the internal non-Gaussian operation on the phase sensitivity and the quantum Fisher information (QFI) in the presence of photon losses. The remainder of this paper is arranged as follows. Section II outlines the theoretical model of the NCO. Section III delves into phase sensitivity, encompassing both the ideal and internal-photon-loss cases. Section IV centers on the QFI and quantum Cramér-Rao bound (QCRB) [54,55]. Finally, Sec. V provides a comprehensive summary.

## II. MODEL

This section begins with an introduction to the SU(1,1) interferometer, as illustrated in Fig. 1(a). The SU(1,1) interferometer typically consists of two OPAs and a linear phase

shifter, making it one of the most commonly used interferometers in quantum metrology research. The first OPA is characterized by a two-mode squeezing operator  $U_{S_1}(\xi_1) = \exp(\xi_1^* ab - \xi_1 a^\dagger b^\dagger)$ , where  $a$  and  $b$  and  $a^\dagger$  and  $b^\dagger$  represent the photon annihilation and creation operators, respectively. The squeezing parameter  $\xi_1$  can be expressed as  $\xi_1 = g_1 e^{i\theta_1}$ , where  $g_1$  represents the gain factor and  $\theta_1$  represents the phase shift. This parameter plays a critical role in shaping the interference pattern and determining the system's phase sensitivity. Following the first OPA, mode  $a$  undergoes a phase shift process  $U_\phi = \exp[i\phi(a^\dagger a)]$ , while mode  $b$  remains unchanged. Subsequently, the two beams are coupled in the second OPA with the operator  $U_{S_2}(\xi_2) = \exp(\xi_2^* ab - \xi_2 a^\dagger b^\dagger)$ , where  $\xi_2 = g_2 e^{i\theta_2}$  and  $\theta_2 - \theta_1 = \pi$ . In this paper, we set the parameters  $g_1 = g_2 = g$ ,  $\theta_1 = 0$ , and  $\theta_2 = \pi$ . We utilize the coherent state  $|\alpha\rangle_a$  and the vacuum state  $|0\rangle_b$  as input states, and homodyne detection is employed on mode  $a$  of the output.

The SU(1,1) interferometer is generally susceptible to photon losses, particularly in the case of internal losses. To simulate photon losses, the use of fictitious BSs is proposed, as depicted in Fig. 1(a). The operators of these fictitious BSs can be represented as  $U_B = U_{B_a} \otimes U_{B_b}$ , with  $U_{B_a} = \exp[\theta_a(a^\dagger a_v - a a_v^\dagger)]$  and  $U_{B_b} = \exp[\theta_b(b^\dagger b_v - b b_v^\dagger)]$ , where  $a_v$  and  $b_v$  represent vacuum modes. Here,  $T_k$  ( $k = a, b$ ) denotes the transmissivity of the fictitious BSs, associated with  $\theta_k$  through  $T_k = \cos^2 \theta_k \in [0, 1]$ . The value of transmissivity equal to 1 ( $T_k = 1$ ) corresponds to the ideal case without photon losses [53]. In an expanded space, the expression for the output state of the standard SU(1,1) interferometer can be represented as the following pure state:

$$|\Psi_{\text{out}}^0\rangle = U_{S_2} U_\phi U_B U_{S_1} |\psi_{\text{in}}\rangle, \quad (1)$$

where  $|\psi_{\text{in}}\rangle = |\alpha\rangle_a |0\rangle_b |0\rangle_{a_v} |0\rangle_{b_v}$ .

To mitigate the impact of photon losses, we introduce a distinct non-Gaussian operation inside the SU(1,1) interferometer, called the NCO scheme, as illustrated in Fig. 1(b). We utilize simple and easy-to-prepare input states ( $|\alpha\rangle_a \otimes |0\rangle_b$ ) and experimentally feasible homodyne detection. Following Ref. [45], the NCO can be seen as an equivalent operator:

$$U_P = s a a^\dagger + t a^\dagger a, \quad (2)$$

where  $s^2 + t^2 = 1$ , with  $s$  and  $t$  being real numbers, and  $a$  and  $a^\dagger$  are the annihilation operator and creation operator, respectively. From Eq. (2), one can obtain the photon addition then photon subtraction (PA-then-PS)  $a a^\dagger$  and photon subtraction then photon addition (PS-then-PA)  $a^\dagger a$ . The process can be described by operator  $U_{P_j}$ , where  $j = 1$  and  $2$ ;  $U_{P_1} = a a^\dagger$ , and  $U_{P_2} = a^\dagger a$ . Actually, the NCOs  $a a^\dagger$  and  $a^\dagger a$  are non-Gaussian operations, which can be experimentally realized via conditional measurement, like  $a$  and  $a^\dagger$ . For instance, on the basis of a BS with high transmissivity and photon detection, one can arrive at the experimental implementation of a single PS [48]. In addition, PA operation can be implemented by a BS with zero photon detection and a single-photon input [56,57]. When the two consecutive conditional measurements are achieved, the quantum state corresponding to the detected results is selected to be our study object. In the ideal case, the

obtained state is not a mixed state but a pure one for a pure input.

In this case of the NCO applied inside the SU(1,1) interferometer, the output state can be written as the following pure states:

$$|\Psi_{\text{out}}^1\rangle = A_1 U_{S_2} U_\phi U_{p_1} U_B U_{S_1} |\psi_{\text{in}}\rangle \quad (3)$$

and

$$|\Psi_{\text{out}}^2\rangle = A_2 U_{S_2} U_\phi U_{p_2} U_B U_{S_1} |\psi_{\text{in}}\rangle. \quad (4)$$

$A_1$  and  $A_2$  are the normalization constants for the PA-then-PS and PS-then-PA schemes, respectively, given by [53]

$$A_1 = (P_{2,2,0,0} + 3P_{1,1,0,0} + 1)^{-\frac{1}{2}}, \quad (5)$$

$$A_2 = (P_{2,2,0,0} + P_{1,1,0,0})^{-\frac{1}{2}}, \quad (6)$$

where  $P_{x_1, y_1, x_2, y_2} = \partial^{x_1+y_1+x_2+y_2} / \partial \lambda_1^{x_1} \partial \lambda_2^{y_1} \partial \lambda_3^{x_2} \partial \lambda_4^{y_2}$   $\{e^{w_4}\}$   $|\lambda_1=\lambda_2=\lambda_3=\lambda_4=0$ , with

$$w_1 = \lambda_1 T (\lambda_2 \sinh g - \lambda_3 \cosh g) \sinh g + \lambda_4 T (\lambda_3 \sinh g - \lambda_2 \cosh g) \sinh g, \quad (7)$$

$$w_2 = \lambda_1 \sqrt{T} \cosh g - \lambda_4 \sqrt{T} \sinh g, \quad (8)$$

$$w_3 = \lambda_2 \sqrt{T} \cosh g - \lambda_3 \sqrt{T} \sinh g, \quad (9)$$

$$w_4 = w_1 + w_2 \alpha^* + w_3 \alpha. \quad (10)$$

### III. PHASE SENSITIVITY

Quantum metrology is an effective approach utilizing quantum resources for precise phase measurements [58,59]. The objective is to achieve highly sensitive measurements of unknown phases. In this section, we delve further into investigating the phase sensitivity for the NCO inside the SU(1,1) interferometer [60]. Various detection methods are available for this purpose, such as homodyne detection [61,62], parity detection [16,63], and intensity detection [64]. Each of these methods offers different trade-offs between sensitivity, complexity, and practical implementation. It is important to note that the phase sensitivities of different detection schemes may vary for different input states and interferometers [65]. Each measurement method has its own advantages. In many schemes, parity detection has been proven to be the optimal detection method for linear phase estimation [16,19], but it is relatively complex and is harder to implement experimentally. Reference [61] noted that the phase sensitivity of an SU(1,1) interferometer with homodyne detection surpasses that with intensity detection. Homodyne detection is not only easy to implement with current experimental technology [56] but also simple from a theoretical-calculation perspective, thereby playing a key role in the field of continuous-variable quantum key distribution [66,67]. For this reason, we use homodyne detection on mode  $a$  at one output port to estimate the phase sensitivity.

In homodyne detection, the measured variable is one of the two orthogonal components of mode  $a$ , given by  $X = (a + a^\dagger)/\sqrt{2}$ . Based on the error-propagation equation [22],

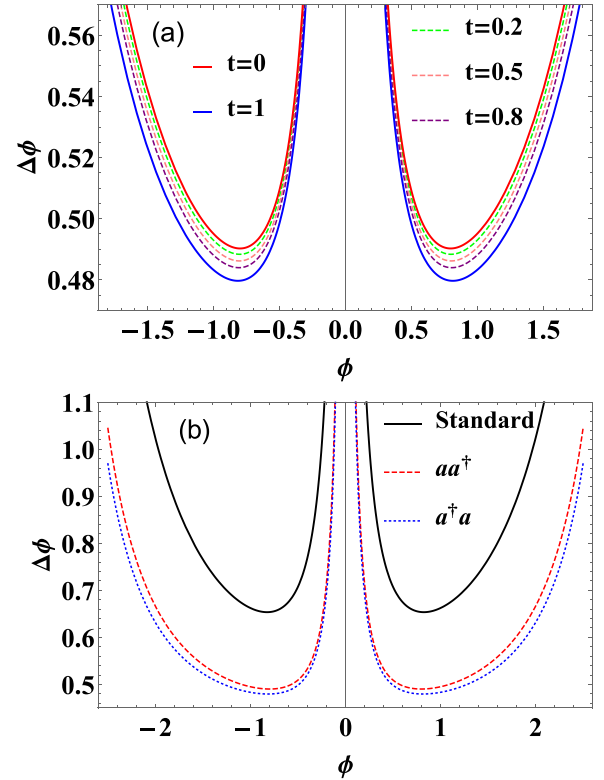


FIG. 2. The phase sensitivity of the NCO based on the homodyne detection as a function of  $\phi$  with  $\alpha = 1$  and  $g = 1$ . (a) The phase sensitivity for different values of the parameter  $t$ . (b) The black solid line corresponds to the standard SU(1,1) interferometer; the red dashed line and the blue dotted line correspond to the PA-then-PS and PS-then-PA schemes, respectively.

the phase sensitivity can be expressed as

$$\Delta\phi = \frac{\sqrt{\langle \Delta^2 X \rangle}}{|\partial \langle X \rangle / \partial \phi|} = \frac{\sqrt{\langle X^2 \rangle - \langle X \rangle^2}}{|\partial \langle X \rangle / \partial \phi|}. \quad (11)$$

Based on Eqs. (3), (4), and (11), the phase sensitivity of the NCO can be theoretically determined. Detailed calculation steps for the phase sensitivity  $\Delta\phi$  of the PA-then-PS and PS-then-PA schemes are provided in Appendix A.

#### A. Ideal case

Initially, we consider the ideal case,  $T_k = 1$  (where  $k = a, b$ ), representing the scenario without photon losses. The phase sensitivity  $\Delta\phi$  is plotted as a function of  $\phi$  in Fig. 2. Figure 2(a) shows different superposition operations, from which it is observed that when  $0 < t < 1$  (dashed lines), the phase sensitivity consistently falls between the extremes of  $t = 0$  (red solid line) and  $t = 1$  (blue solid line), which correspond to the PA-then-PS and PS-then-PA schemes, respectively. This indicates that the effects of superposition operations are between the PS-then-PA and PA-then-PS schemes in the improvement of phase sensitivity. Thus, for the sake of simplicity, our subsequent investigation concentrates only on these two boundary cases. Figure 2(b) shows the standard case and these two boundary cases. The following is shown: (1) The phase sensitivity improves initially and then

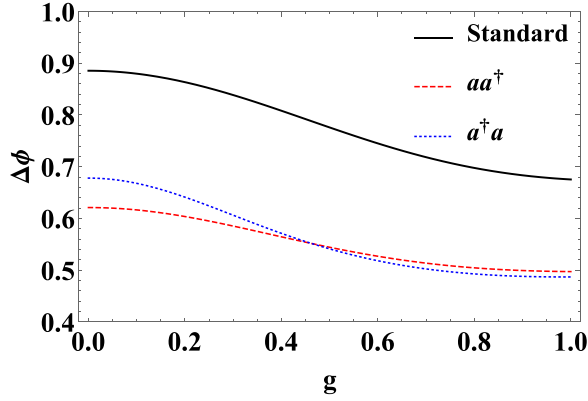


FIG. 3. The phase sensitivity as a function of  $g$ , with  $\alpha = 1$  and  $\phi = 0.6$ .

decreases as the phase increases, with the optimal sensitivity deviating from  $\phi = 0$ . (2) Both the PA-then-PS and PS-then-PA schemes effectively enhance the phase sensitivity  $\Delta\phi$ . (3) The phase sensitivity of the PS-then-PA scheme is better than that of the PA-then-PS scheme, and the difference increases with increasing phase.

Figure 3 illustrates that the phase sensitivity  $\Delta\phi$  plotted against the gain factor  $g$  for different schemes. The plot confirms that an increase in the gain factor  $g$  enhances the phase sensitivity. It is interesting to notice that, when the  $g$  value is small, the PA-then-PS scheme demonstrates greater improvement. Conversely, when the  $g$  value is large, the opposite is true. Although the improvement of both is related to the parameter  $g$ , the PS-then-PA scheme is better in terms of accuracy; i.e., the PS-then-PA scheme achieves the optimal phase sensitivity. Thus, the following studies mainly focus on large values of the parameter  $g$ .

Similarly, we analyze the phase sensitivity  $\Delta\phi$  as a function of the coherent amplitude  $\alpha$ , as depicted in Fig. 4. The phase sensitivity improves with the coherent amplitude  $\alpha$ , attributed to the increase in the mean photon number with  $\alpha$ , which enhances intramode correlations and quantum entanglement between the two modes. Furthermore, the enhancement effect diminishes as the coherent amplitude  $\alpha$  increases. It is noteworthy that the PS-then-PA

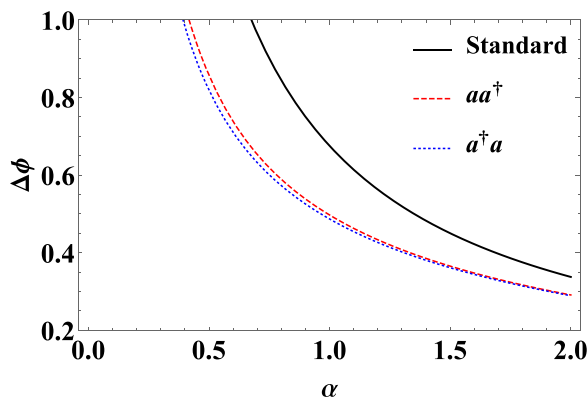


FIG. 4. The phase sensitivity as a function of  $\alpha$ , with  $g = 1$  and  $\phi = 0.6$ .

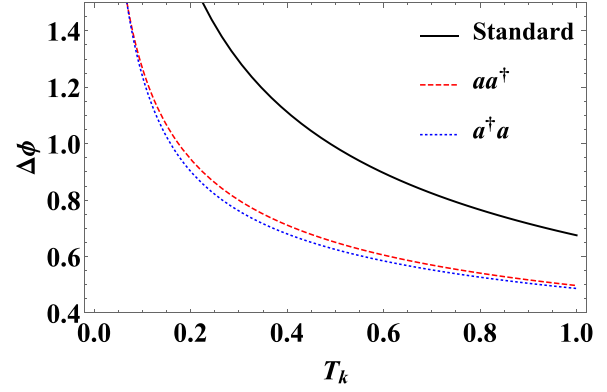


FIG. 5. The phase sensitivity as a function of transmittance  $T_k$ , with  $g = 1$ ,  $\phi = 0.6$ , and  $\alpha = 1$ .

scheme demonstrates greater improvement than the PA-then-PS scheme at small values of  $\alpha$ , while the improvement effects of both schemes are consistent at larger values of  $\alpha$ .

## B. Photon-loss case

The SU(1,1) interferometer plays a critical role in achieving high-precision measurements. However, precision is significantly affected by photon losses, particularly internal losses. Here, we focus on internal photon losses, corresponding to  $T_k \in (0, 1)$ . The phase sensitivity, depicted as a function of the transmittance  $T_k$  in Fig. 5 for fixed  $g$ ,  $\alpha$ , and  $\phi$ , improves as anticipated with higher transmittance  $T_k$ . Lower transmittance corresponds to increased internal losses, weakening the performance of phase estimation. Both the PA-then-PS and PS-then-PA schemes within the SU(1,1) interferometer effectively enhance the phase sensitivity  $\Delta\phi$ . Moreover, it is notable that as transmittance  $T_k$  increases, the improvement in phase sensitivity first increases and then decreases for both schemes. Notably, the PS-then-PA scheme consistently demonstrates higher phase sensitivity than the PA-then-PA scheme across the entire range.

The robustness to photon losses denotes the measurement process's insensitivity to photon losses. A quantum precision measurement system with strong robustness can maintain high accuracy and stability even in the presence of photon losses, thereby reducing measurement errors and uncertainties. By designing and optimizing interferometer measurement processes, the system's robustness to photon losses can be improved.

To better study the enhancing effect of the NCO on robustness against photon losses, we further compare the changes in the phase sensitivity in ideal and photon-loss cases for different schemes in Fig. 6. The comparison reveals that the phase sensitivity of the standard SU(1,1) interferometer is more significantly affected by photon losses. In contrast, the phase sensitivity of the NCO is less affected, indicating that the non-Gaussian operations can mitigate the impact of internal photon losses and enhance the interferometer's robustness against losses.

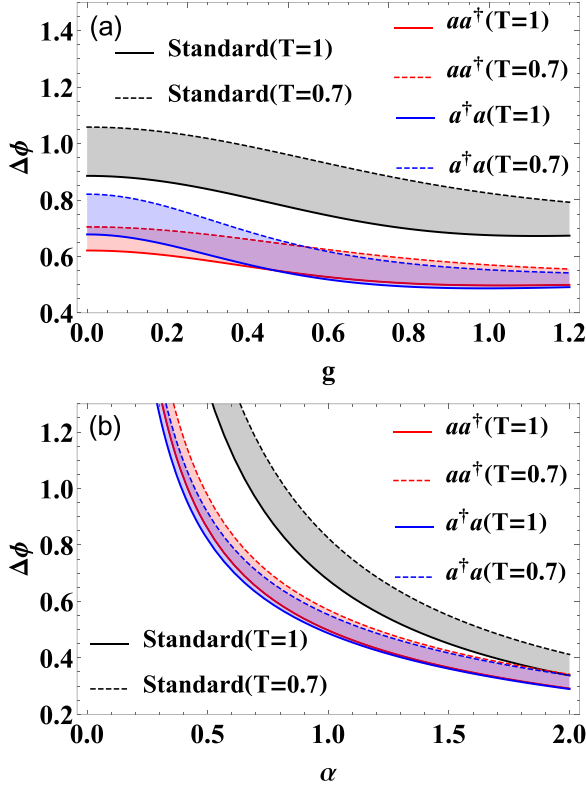


FIG. 6. Comparisons of robustness against photon losses. (a) The phase sensitivity as a function of  $g$ , with  $\alpha = 1$  and  $\phi = 0.6$ . (b) The phase sensitivity as a function of  $\alpha$ , with  $g = 1$  and  $\phi = 0.6$ .

### C. Comparison with the SQL and HL

Additionally, we compare the phase sensitivity with the SQL and HL in this section. The SQL and HL are defined as  $\Delta\phi_{\text{SQL}} = 1/\sqrt{N_j}$  and  $\Delta\phi_{\text{HL}} = 1/N_j$ , respectively. Here,  $N_j$  represents the total mean photon number inside the interferometer before the second OPA for each scheme [10,68], with  $j = 1$  or  $2$ .  $N_j$  can be calculated as

$$\begin{aligned} N_1 &= A_1^2 \langle \psi_{\text{in}} | U_{S_1}^\dagger U_B^\dagger U_{P_1}^\dagger (a^\dagger a + b^\dagger b) U_{P_1} U_B U_{S_1} | \psi_{\text{in}} \rangle \\ &= A_1^2 (P_{3,3,0,0} + 5P_{2,2,0,0} + 4P_{1,1,0,0} \\ &\quad + P_{2,2,1,1} + 3P_{1,1,1,1} + P_{0,0,1,1}) \end{aligned} \quad (12)$$

for the PA-then-PS scheme and

$$\begin{aligned} N_2 &= A_2^2 \langle \psi_{\text{in}} | U_{S_1}^\dagger U_B^\dagger U_{P_2}^\dagger (a^\dagger a + b^\dagger b) U_{P_2} U_B U_{S_1} | \psi_{\text{in}} \rangle \\ &= A_2^2 (P_{3,3,0,0} + 3P_{2,2,0,0} + P_{1,1,0,0} \\ &\quad + P_{2,2,1,1} + P_{1,1,1,1}) \end{aligned} \quad (13)$$

for the PS-then-PA scheme.

For these two schemes at fixed  $g$  and  $\alpha$ , we plot the phase sensitivity  $\Delta\phi$  as a function of  $\phi$  for comparison with the SQL and the HL of the standard SU(1,1) interferometer. Our findings demonstrate the following: (1) The original interferometer (without NCO) cannot surpass the SQL. (2) The NCO schemes are capable of surpassing the SQL within a wide range, even in the presence of significant photon losses [Fig. 7(b)]. This suggests that the NCO schemes show greater robustness against internal photon losses. (3) The phase

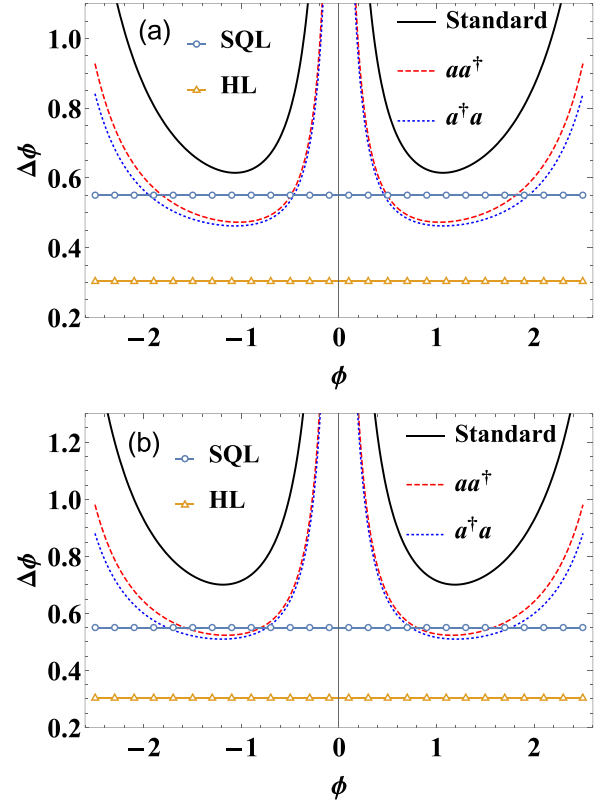


FIG. 7. Comparison of phase sensitivity with the SQL and HL for fixed  $g = 0.7$  and  $\alpha = 1$ . The blue circles show the SQL, and the yellow triangles show the HL. (a)  $T = 1$  and (b)  $T = 0.7$ .

sensitivity of the PS-then-PA scheme is better than that of the PA-then-PS scheme.

## IV. THE QUANTUM FISHER INFORMATION

In the previous discussion, we explored the influence of NCO schemes on phase sensitivity and the correlation between phase sensitivity and relevant parameters using homodyne detection. It is crucial to recognize that the discussed phase sensitivity is influenced by the chosen measurement method. Hence, the question arises: how can we achieve maximum phase sensitivity in an interferometer that is independent of the measurement method used? This section shifts our focus to the QFI, which represents the maximum information extracted from the interferometer system, regardless of the measurement method employed. We will examine the QFI in ideal and realistic scenarios.

### A. Ideal case

For a pure-state system, the QFI can be derived by [69]

$$F_j = 4[\langle \Psi'_j | \Psi'_j \rangle - |\langle \Psi'_j | \Psi_j \rangle|^2], \quad (14)$$

where  $|\Psi_j\rangle$  is the quantum state after the phase shift and before the second OPA and  $|\Psi'_j\rangle = \partial|\Psi_j\rangle/\partial\phi$ . Then the QFI can be rewritten as [69]

$$F_j = 4\langle \Delta^2 n_a \rangle, \quad (15)$$

where  $\langle \Delta^2 n_a \rangle = \langle \Psi_j | (a^\dagger a)^2 | \Psi_j \rangle - (\langle \Psi_j | a^\dagger a | \Psi_j \rangle)^2$ .

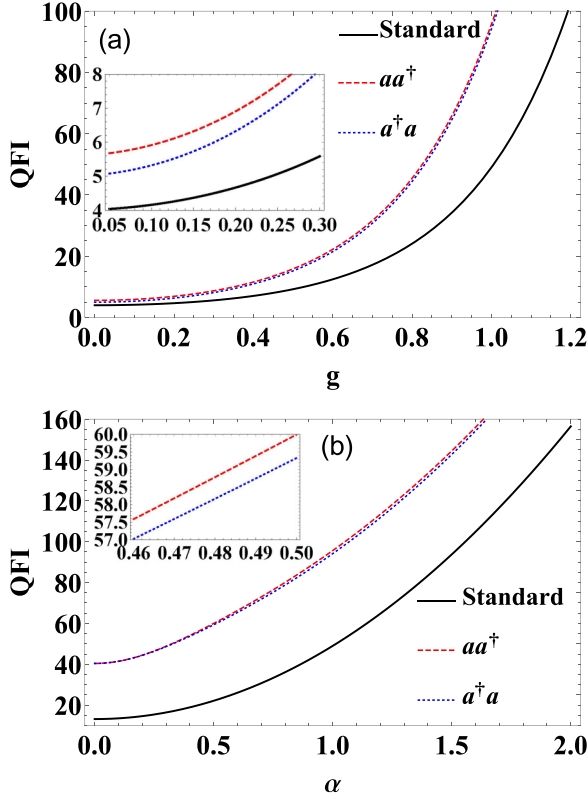


FIG. 8. (a) The QFI as a function of  $g$ , with  $\alpha = 1$ . (b) The QFI as a function of  $\alpha$ , with  $g = 1$ .

In the ideal NCO, the quantum state is given by  $|\Psi_j\rangle = A_j U_\phi U_{p_j} U_{S_j} |\alpha\rangle_a |0\rangle_b$ , with  $U_{P_1} = aa^\dagger$  ( $j = 1$ ) and  $U_{P_2} = a^\dagger a$  ( $j = 2$ ). Thus, the QFI is derived as

$$F_1 = 4 \left\{ A_1^2 (P_{4,4,0,0} + 8P_{3,3,0,0} + 14P_{2,2,0,0} + 4P_{1,1,0,0}) - [A_1^2 (P_{3,3,0,0} + 5P_{2,2,0,0} + 4P_{1,1,0,0})]^2 \right\} \quad (16)$$

for the PA-then-PS scheme and

$$F_2 = 4 \left\{ A_2^2 (P_{4,4,0,0} + 6P_{3,3,0,0} + 7P_{2,2,0,0} + P_{1,1,0,0}) - [A_2^2 (P_{3,3,0,0} + 3P_{2,2,0,0} + P_{1,1,0,0})]^2 \right\} \quad (17)$$

for the PS-then-PA scheme. In the above equations,  $T_k = 1$ . It is possible to explore the connection between the QFI and the related parameters using Eqs. (16) and (17).

Figure 8 illustrates the QFI as a function of  $g$  ( $\alpha$ ) for a specific  $\alpha$  ( $g$ ). It is evident that a higher value of  $g$  ( $\alpha$ ) corresponds to greater QFI. Both the PA-then-PS and PS-then-PA schemes result in enhanced QFI due to the non-Gaussian nature. The QFI of the PA-then-PS scheme is slightly higher than that of the PS-then-PA scheme in both plots. Moreover, we observe that the improvement in QFI due to non-Gaussian operations increases with the increase of  $g$  [as shown in Fig. 8(a)], while it does not significantly change with the variation of the value of  $\alpha$  [as shown in Fig. 8(b)].

Actually, the QFI can be associated with the phase sensitivity through [70]

$$\Delta\phi_{\text{QCRB}} = \frac{1}{\sqrt{vF}}, \quad (18)$$

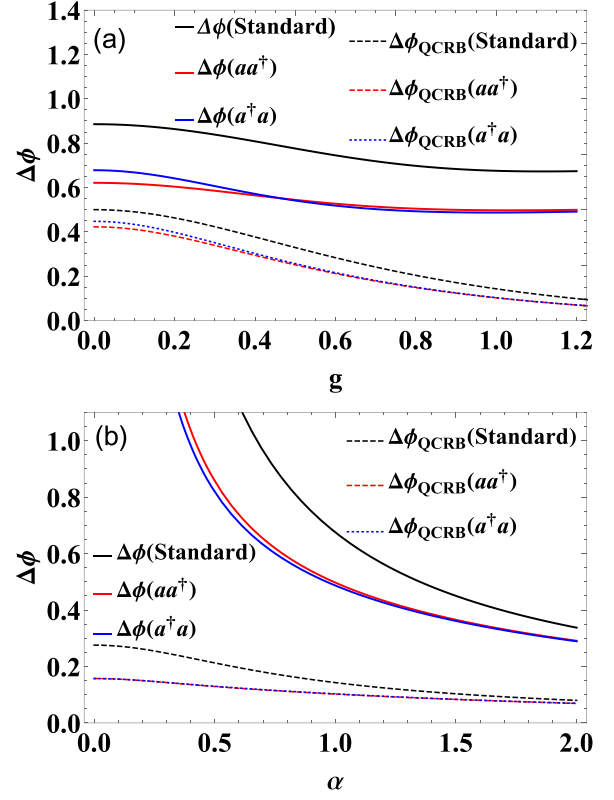


FIG. 9. Comparisons of the phase sensitivity  $\Delta\phi$  obtained by homodyne detection with the ultimate sensitivity  $\Delta\phi_{\text{QCRB}}$  obtained from QFI.

where  $v$  represents the number of measurements. For simplicity, we set  $v = 1$ . Another quantum limit, the QCRB [54,55], denoted as  $\Delta\phi_{\text{QCRB}}$ , defines the ultimate limit for a set of probabilities derived from measurements on a quantum system. It is an estimator implemented asymptotically by a maximum-likelihood estimator and provides detection-independent phase sensitivity. In order to better help us understand how optimal the phase sensitivity obtained from the SU(1,1) interferometer with the NCO really is, we compare the phase sensitivity  $\Delta\phi$  obtained by using the second OPA and homodyne detection with the sensitivity  $\Delta\phi_{\text{QCRB}}$  obtained from the QFI. Figure 9 illustrates the variation of  $\Delta\phi_{\text{QCRB}}$  as a function of  $g$  ( $\alpha$ ) for a specific  $\alpha$  ( $g$ ). It shows that  $\Delta\phi_{\text{QCRB}}$  improves with increasing  $g$  and  $\alpha$ . Similarly, due to the non-Gaussian nature, both the PA-then-PS and PS-then-PA schemes are able to improve  $\Delta\phi_{\text{QCRB}}$ . Furthermore, the improvement in  $\Delta\phi_{\text{QCRB}}$  is more obvious for a small coherent amplitude  $\alpha$  [see Fig. 9(b)]. It is shown that for a smaller gain factor or a greater coherent amplitude, the measurement-based sensitivity better reflects the Fisher-information situation (described via  $\Delta\phi_{\text{QCRB}}$ ).

## B. Photon-loss case

In this section, we extend our analysis to cover the QFI in the presence of photon losses. Specifically, we examine homodyne detection on mode  $a$ , which is susceptible to photon losses. Consequently, our attention is directed toward the QFI of the system with photon losses in mode  $a$ , as depicted

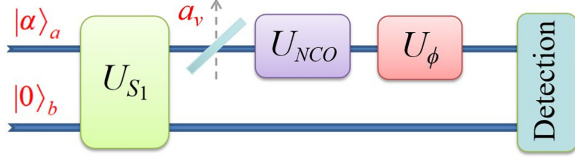


FIG. 10. Schematic diagram of the photon losses in mode  $a$ . The losses occur before the NCO.

in Fig. 10. Here, we should emphasize that the Fisher information is obtained using the state preceding the second OPA; i.e., despite Fig. 10 featuring an SU(1,1) interferometer diagram, the second OPA is not essential. For realistic quantum systems, we demonstrate the feasibility of computing the QFI with internal non-Gaussian operations according to the method proposed by Escher *et al.* [69]. See Appendix B for the detailed process. The method is briefly summarized as follows.

For the case of photon losses, we can treat the system as a pure state in an extended space, similar to Eq. (3). Then following Eq. (14), we can obtain the QFI under the pure state, denoted as  $C_{Q_j}$ , which is larger than or equal to the QFI  $F_{L_j}$  for the mixed state (our consideration), i.e.,  $F_{L_j} \leq C_{Q_j}$ .  $C_{Q_j}$  is the QFI before optimizing over all possible measurements, i.e.,

$$C_{Q_j} = 4[\langle \psi | \hat{H}_{1_j} | \psi \rangle - |\langle \psi | \hat{H}_{2_j} | \psi \rangle|^2], \quad (19)$$

where  $\hat{H}_{1_j}$  and  $\hat{H}_{2_j}$  are defined as

$$\hat{H}_{1_j} = B_j^2 \sum_{l=0}^{\infty} \frac{d}{d\phi} \Pi_l^\dagger(\eta, \phi, \lambda) U_{p_j}^\dagger U_{p_j} \frac{d}{d\phi} \Pi_l(\eta, \phi, \lambda), \quad (20)$$

$$\hat{H}_{2_j} = iB_j^2 \sum_{l=0}^{\infty} \left[ \frac{d}{d\phi} \Pi_l^\dagger(\eta, \phi, \lambda) \right] U_{p_j}^\dagger U_{p_j} \Pi_l(\eta, \phi, \lambda). \quad (21)$$

Here,  $B_j$  are normalization factors shown in Eq. (B10), and  $\Pi_l(\eta, \phi, \lambda)$  is the phase-dependent Krause operator shown in Eq. (B8), satisfying  $\sum \Pi_l^\dagger(\eta, \phi, \lambda) \Pi_l(\eta, \phi, \lambda) = 1$ , with  $\lambda = 0$  and  $\lambda = -1$  representing the photon losses before the phase shifter and after the phase shifter, respectively.  $\eta$  is related to the dissipation factor, with  $\eta = 1$  and  $\eta = 0$  being the cases of complete loss and absorption, respectively. Particularly, Eqs. (19), (20), and (21) just reduce to those in Ref. [69] when there are no non-Gaussian operations. Following the spirit of Ref. [69], we can further obtain the minimum value of  $C_{Q_j}$  by optimizing over  $\lambda$ , corresponding to  $F_{L_j}$ , i.e.,  $F_{L_j} = \min_{\Pi_l(\eta, \phi, \lambda)} C_{Q_j} \leq C_{Q_j}$ . See Appendix B for more details.

Next, we further analyze the effects of each parameter on the QFI of the NCO schemes under photon loss by numerical calculation. Figure 11 plots the QFI and QCRB as a function of transmittance  $\eta$ , from which it is observed that the QFI increases with increasing transmittance  $\eta$ , and the NCO can enhance the QFI. This increase can be attributed to the NCO increasing the number of photons internally, resulting in more quantum information, similar to the ideal case. For both non-Gaussian operations, the improved QFI increases with the transmittance  $\eta$ . It is interesting that, over a wide range of about  $0 < \eta < 0.85$ , the PS-then-PA scheme exhibits more QFI or higher precision than the PA-then-PS scheme. However, as  $\eta$  approaches 1, the PA-then-PS scheme demonstrates superior QFI or QCRB within the range of about

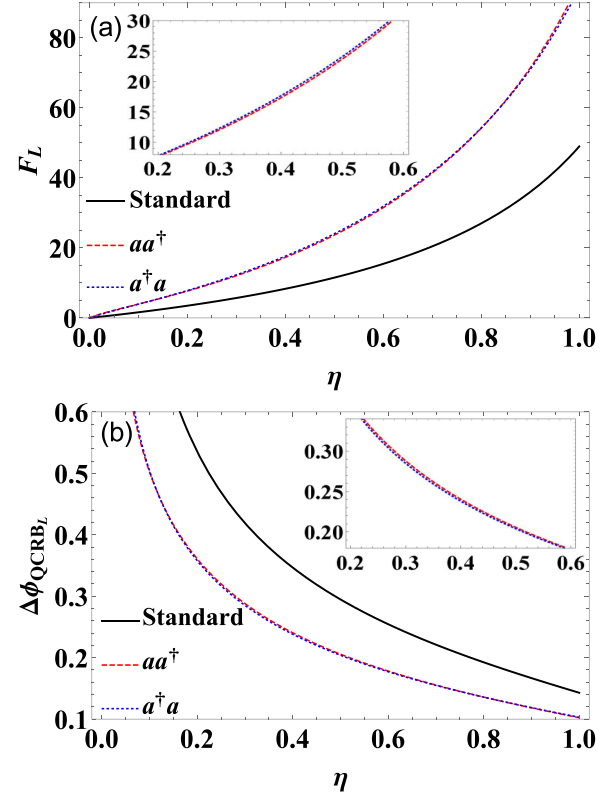


FIG. 11.  $F_L$  and  $\Delta\phi_{\text{QCRB}_L}$  as a function of transmittance  $\eta$ , with  $g = 1$  and  $\alpha = 1$ .

$0.85 < \eta < 1$ . This implies that the PS-then-PA scheme presents better performance than the PA-then-PS scheme in the high-dissipation situation.

To explore the underlying reasons for the above case, we further examine the nonclassicality of the NCO using the negative volume of the Wigner function (WF) [71]. For simplicity, we consider only the WF of ideal quantum states after non-Gaussian operations. Some details of the WF are summarized in Appendix C. Figure 12 illustrates the WF in phase space corresponding to two different operations. It is clear that (1) both non-Gaussian operations can increase the negative

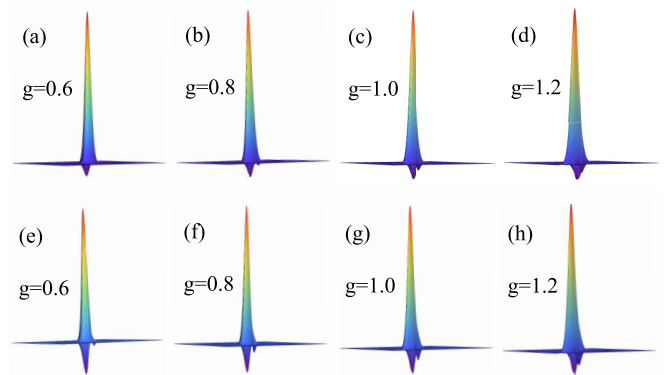


FIG. 12. The WF in phase space for quantum states after the NCO with  $\alpha = 1$ . (a)–(d) The PA-then-PS scheme and (e)–(h) the PS-then-PA scheme, with  $g = 0.6, 0.8, 1.0, 1.2$  (from left to right).

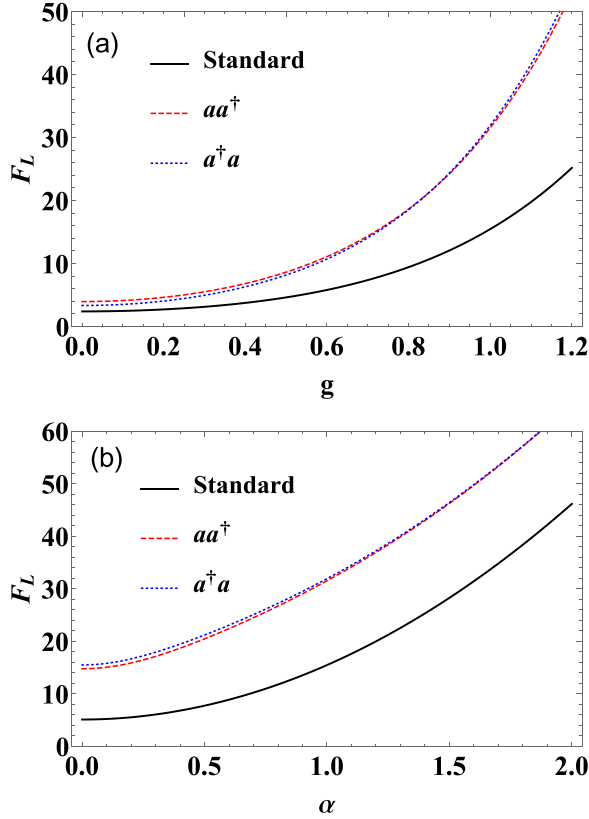


FIG. 13. (a)  $F_L$  as a function of  $g$ , with  $\alpha = 1$  and  $\eta = 0.6$ . (b)  $F_L$  as a function of  $\alpha$ , with  $g = 1$  and  $\eta = 0.6$ .

volume of the WF, i.e., increase the nonclassicality [71], and (2) for given  $\alpha$  and  $g$ , the PS-then-PA scheme presents a much bigger negative volume than the PA-then-PS scheme. For example, for  $\alpha = 1$  and  $g = 0.6, 0.8, 1.0, 1.2$ , the negative volumes are 0.034 and 0.009, 0.033 and 0.014, 0.031 and 0.017, and 0.030 and 0.020 for the PS-then-PA and PA-then-PS schemes, respectively. These observations suggest that the non-Gaussian operation increases the nonclassicality, and the stronger the nonclassicality of the internal non-Gaussian operation is, the more effective it is in suppressing the effect of the internal high noise.

Similar to the ideal case, Fig. 13 illustrates the QFI as a function of  $g$  ( $\alpha$ ) for a given  $\alpha$  ( $g$ ) for the loss case with  $\eta = 0.6$ . Some results similar to those in Fig. 8 can be obtained (not shown here). Different from the ideal case in Fig. 8, the PS-then-PA scheme performs better than PA-then-PS scheme when  $g$  is larger, as shown in Fig. 13(a). This case is also true for the QFI with  $\alpha$ , as shown in Fig. 13(b). These two cases are almost the opposite of the previous ideal situation. The reason may be that the PS-then-PA operation prepares the higher nonclassical states, which are more conducive to improving the measurement accuracy, especially in the presence of high photon losses.

## V. CONCLUSION

In this paper, we analyzed the effects of NCO schemes on the phase sensitivity, the QFI, and the QCRB in both ideal and photon-loss cases. Additionally, we investigated the effects of

the gain coefficient  $g$  of the OPA, the coherent-state amplitude  $\alpha$ , and the transmittance  $T_k$  of the BS on the performance of the system. Through analytical comparison, we verified that the NCO schemes can improve the measurement accuracy of the SU(1,1) interferometer and enhance the robustness against internal photon losses. The non-Gaussian operations can elevate the total mean photon number of the SU(1,1) interferometer, consequently reinforcing intramode correlations and quantum entanglement between the two modes.

We further analyzed the differences between the two non-Gaussian operations. Concerning the phase sensitivity, the improvement of the PS-then-PA scheme is superior in both the ideal and photon-loss cases. In terms of the QFI and QCRB, in the ideal case, the PA-then-PS scheme slightly outperforms the PS-then-PA scheme. However, in the photon-loss case, the PS-then-PA scheme demonstrates a greater advantage.

In summary, the NCO schemes play a role in overcoming the internal photon losses within SU(1,1) interferometers and in improving the accuracy of quantum measurements. This study highlights the potential of the non-Gaussian operations as valuable tools for improving the performance of quantum metrology and information-processing systems. It should be noted that we mainly paid attention to an ideal PS or PA case. Actually, there are some methods to realize these operations. The different experimental parameters will impact the performance, which will be further examined in the near future.

## ACKNOWLEDGMENTS

This work is supported by the National Natural Science Foundation of China (Grants No. 11964013 and No. 12104195) and the Key Project of the Natural Science Foundation of Jiangxi Province, Jiangxi Provincial Key Laboratory of Advanced Electronic Materials and Devices (Grant No. 2024SSY03011).

## APPENDIX A: THE PHASE SENSITIVITY WITH THE NCO

In this Appendix, we give the calculation formulas of the phase sensitivity with the NCO as follows:

$$\Delta\phi_1 = \frac{\sqrt{\langle \Psi_{\text{out}}^1 | (a^\dagger + a)^2 | \Psi_{\text{out}}^1 \rangle - \langle \Psi_{\text{out}}^1 | (a^\dagger + a) | \Psi_{\text{out}}^1 \rangle^2}}{|\partial \langle \Psi_{\text{out}}^1 | (a^\dagger + a) | \Psi_{\text{out}}^1 \rangle / \partial \phi|}. \quad (\text{A1})$$

Here, the output state  $|\Psi_{\text{out}}^1\rangle$  is given by Eq. (3), so the expectations related to the phase sensitivity in PA-then-PS scheme are specifically calculated as follows [53]:

$$\begin{aligned} & \langle \Psi_{\text{out}}^1 | (a^\dagger + a) | \Psi_{\text{out}}^1 \rangle \\ &= A_1^2 [e^{-i\phi} \cosh g (P_{3,2,0,0} + 4P_{2,1,0,0} + 2P_{1,0,0,0}) \\ & \quad + \sinh g (P_{2,2,0,1} + 3P_{1,1,0,1} + P_{0,0,0,1}) \\ & \quad + e^{i\phi} \cosh g (P_{2,3,0,0} + 4P_{1,2,0,0} + 2P_{0,1,0,0}) \\ & \quad + \sinh g (P_{2,2,1,0} + 3P_{1,1,1,0} + P_{0,0,1,0})] \end{aligned} \quad (\text{A2})$$

and

$$\begin{aligned} & \langle \Psi_{\text{out}}^1 | (a^\dagger + a)^2 | \Psi_{\text{out}}^1 \rangle \\ &= A_1^2 [e^{-2i\phi} \cosh^2 g (P_{4,2,0,0} + 5P_{3,1,0,0} + 3P_{2,0,0,0}) \end{aligned}$$



$$\begin{aligned}
& \times e^{2i\phi} \cosh^2 g(P_{2,4,0,0} + 5P_{1,3,0,0} + 3P_{0,2,0,0}) \\
& + 2 \cosh^2 g(P_{3,3,0,0} + 5P_{2,2,0,0} + 4P_{1,1,0,0}) \\
& + 2e^{-i\phi} \sinh g \cosh g(P_{3,2,0,1} + 4P_{2,1,0,1} \\
& + 2P_{1,0,0,1} + P_{3,2,1,0} + 4P_{2,1,1,0} + 2P_{1,0,1,0}) \\
& + 2e^{i\phi} \sinh g \cosh g(P_{2,3,1,0} + 4P_{1,2,1,0} \\
& + 2P_{0,1,1,0} + P_{2,3,0,1} + 4P_{1,2,0,1} + 2P_{0,1,0,1}) \\
& + \sinh^2 g(P_{2,2,0,2} + 3P_{1,1,0,2} + P_{0,0,0,2} \\
& + P_{2,2,2,0} + 3P_{1,1,2,0} + P_{0,0,2,0} + 2P_{2,2,1,1} \\
& + 6P_{1,1,1,1} + 2P_{0,0,1,1} + 2P_{2,2,0,0} \\
& + 6P_{1,1,0,0} + 2) + A_1^{-2}. \tag{A3}
\end{aligned}$$

The phase sensitivity in the PS-then-PA scheme can be calculated as

$$\Delta\phi_2 = \frac{\sqrt{\langle \Psi_{\text{out}}^2 | (a^\dagger + a)^2 | \Psi_{\text{out}}^2 \rangle - \langle \Psi_{\text{out}}^2 | (a^\dagger + a) | \Psi_{\text{out}}^2 \rangle^2}}{|\partial \langle \Psi_{\text{out}}^2 | (a^\dagger + a) | \Psi_{\text{out}}^2 \rangle / \partial \phi|}, \tag{A4}$$

where the output state  $|\Psi_{\text{out}}^2\rangle$  is given by Eq. (4), and the expectations associated with the phase sensitivity in the PS-then-PA scheme can similarly be calculated as follows:

$$\begin{aligned}
& \langle \Psi_{\text{out}}^2 | (a^\dagger + a) | \Psi_{\text{out}}^2 \rangle \\
& = A_2^2 [e^{-i\phi} \cosh g(P_{3,2,0,0} + 2P_{2,1,0,0}) \\
& + \sinh g(P_{2,2,0,1} + P_{1,1,0,1}) \\
& + e^{i\phi} \cosh g(P_{2,3,0,0} + 2P_{1,2,0,0}) \\
& + \sinh g(P_{2,2,1,0} + P_{1,1,1,0})] \tag{A5}
\end{aligned}$$

and

$$\begin{aligned}
& \langle \Psi_{\text{out}}^2 | (a^\dagger + a)^2 | \Psi_{\text{out}}^2 \rangle \\
& = A_2^2 [e^{-2i\phi} \cosh^2 g(P_{4,2,0,0} + 3P_{3,1,0,0}) \\
& + e^{2i\phi} \cosh^2 g(P_{2,4,0,0} + 3P_{1,3,0,0}) \\
& + 2 \cosh^2 g(P_{3,3,0,0} + 3P_{2,2,0,0} + P_{1,1,0,0}) \\
& + 2e^{-i\phi} \sinh g \cosh g(P_{3,2,1,0} + 2P_{2,1,1,0} \\
& + P_{3,2,0,1} + 2P_{2,1,0,1}) \\
& + 2e^{i\phi} \sinh g \cosh g(P_{2,3,0,1} + 2P_{1,2,0,1} \\
& + P_{2,3,1,0} + 2P_{1,2,1,0}) \\
& + \sinh^2 g(P_{2,2,2,0} + P_{1,1,2,0} + P_{2,2,0,2} \\
& + P_{1,1,0,2} + 2P_{2,2,1,1} + 2P_{1,1,1,1} \\
& + 2P_{2,2,0,0} + 2P_{1,1,0,0}) + A_2^{-2}]. \tag{A6}
\end{aligned}$$

## APPENDIX B: THE QFI WITH PHOTON LOSSES

Here, we further examine the QFI with photon losses for the system shown in Fig. 10. After the first OPA  $U_{S_1}$ , the photon losses, the non-Gaussian operation  $U_{P_j}$  ( $j = 1$  or  $2$ ), and, before the detection, the output state in an expanded

space are given by

$$|\Psi_{E_j}\rangle = B_j U_\phi U_{P_j} U_B |0\rangle_{a_v} |\psi\rangle, \tag{B1}$$

a form of the pure state, where  $|\psi\rangle = U_{S_1} |\alpha\rangle_a |0\rangle_b$  and  $B_j$  is the normalization factor, determined by  $\text{Tr} |\Psi_{E_j}\rangle \langle \Psi_{E_j}| = 1$ .

For a pure-state system, the QFI can be calculated using Eq. (14) and is denoted  $C_{Q_j}$ . Substituting Eq. (B1) into Eq. (14) yields

$$C_{Q_j} = 4[\langle \psi | \hat{H}_{1_j} | \psi \rangle - |\langle \psi | \hat{H}_{2_j} | \psi \rangle|^2], \tag{B2}$$

where  $\hat{H}_{1_j}$  and  $\hat{H}_{2_j}$  are operators defined as

$$\hat{H}_{1_j} = B_j^2 \langle 0 | \frac{dU_B^\dagger U_{P_j}^\dagger U_\phi^\dagger}{d\phi} \frac{dU_\phi U_{P_j} U_B}{d\phi} | 0 \rangle_{a_v}, \tag{B3}$$

$$\hat{H}_{2_j} = iB_j^2 \langle 0 | \frac{dU_B^\dagger U_{P_j}^\dagger U_\phi^\dagger}{d\phi} U_\phi U_{P_j} U_B | 0 \rangle_{a_v}. \tag{B4}$$

Noticing that  $[U_\phi, U_{P_j}] = 0$ , i.e.,  $U_\phi$  and  $U_{P_j}$  are commutative, and inserting the completeness relation of the number state  $\sum |l\rangle_{a_v, a_v} \langle l| = 1$ , one can obtain

$$\begin{aligned}
\hat{H}_{1_j} & = B_j^2 \sum_{l=0}^{\infty} \langle 0 | \frac{dU_B^\dagger U_{P_j}^\dagger U_\phi^\dagger}{d\phi} | l \rangle_{a_v, a_v} \langle l | \frac{dU_\phi U_{P_j} U_B}{d\phi} | 0 \rangle_{a_v} \\
& = B_j^2 \sum_{l=0}^{\infty} \frac{d}{d\phi} \langle 0 | U_B^\dagger U_\phi^\dagger | l \rangle_{a_v} U_{P_j}^\dagger U_{P_j} \frac{d}{d\phi} \langle l | U_\phi U_B | 0 \rangle_{a_v} \\
& = B_j^2 \sum_{l=0}^{\infty} \frac{d}{d\phi} \Pi_l^\dagger(\eta, \phi) U_{P_j}^\dagger U_{P_j} \frac{d}{d\phi} \Pi_l(\eta, \phi) \tag{B5}
\end{aligned}$$

and

$$\begin{aligned}
\hat{H}_{2_j} & = iB_j^2 \sum_{l=0}^{\infty} \langle 0 | \frac{dU_B^\dagger U_{P_j}^\dagger U_\phi^\dagger}{d\phi} | l \rangle_{a_v, a_v} \langle l | U_\phi U_{P_j} U_B | 0 \rangle_{a_v} \\
& = iB_j^2 \sum_{l=0}^{\infty} \left[ \frac{d}{d\phi} \Pi_l^\dagger(\eta, \phi) \right] U_{P_j}^\dagger U_{P_j} \Pi_l(\eta, \phi), \tag{B6}
\end{aligned}$$

where  $\Pi_l^\dagger(\eta, \phi) = [\Pi_l(\eta, \phi)]^\dagger$  and

$$\begin{aligned}
\Pi_l(\eta, \phi) & = {}_{a_v} \langle l | U_\phi U_B | 0 \rangle_{a_v} \\
& = \sqrt{\frac{(1-\eta)^l}{l!}} e^{i\phi n} \eta^{\frac{n}{2}} a^l. \tag{B7}
\end{aligned}$$

Here,  $\Pi_l(\eta, \phi)$  is actually the Kraus operator, which describes the photon losses and satisfies  $\sum \Pi_l^\dagger(\eta, \phi) \Pi_l(\eta, \phi) = 1$ , and  $n = a^\dagger a$  is the number operator.  $\eta$  is related to the dissipation factor, with  $\eta = 1$  and  $\eta = 0$  being the cases of complete loss and absorption, respectively.

For a pure state in extended space, the quantum Fisher information  $C_{Q_j}$  about the parameter  $\phi$  is larger than or equal to the quantum Fisher information  $F_{L_j}$  for a mixed state, i.e.,  $F_{L_j} \leq C_{Q_j}$ .  $C_{Q_j}$  is the quantum expression for the Fisher in the formation before optimizing over all possible measurements. Following the spirit of Ref. [69], i.e., in an interferometer with photon losses in one arm, a possible set of Kraus operators describing the process is

$$\Pi_l(\eta, \phi, \lambda) = \sqrt{\frac{(1-\eta)^l}{l!}} e^{i\phi(n-\lambda)} \eta^{\frac{n}{2}} a^l, \tag{B8}$$

which also satisfies  $\sum \Pi_l^\dagger(\eta, \phi, \lambda) \Pi_l(\eta, \phi, \lambda) = 1$ . Here,  $\lambda = 0$  and  $\lambda = -1$  represent the photon losses before the phase shifter and after the phase shifter, respectively. Thus, one can obtain  $F_{L_j}$  by optimizing the parameter  $\lambda$  corresponding to all possible measurements, i.e.,

$$F_{L_j} = \min_{\Pi_l(\eta, \phi, \lambda)} C_{Q_j} \leq C_{Q_j}. \quad (\text{B9})$$

In this paper, we use Eqs. (B2), (B8), and (B9) to discuss  $F_{L_j}$  under photon losses by minimizing  $C_{Q_j}$  over  $\lambda$ .

Next, we further derive the normalization factor  $B_j$ . Using Eq. (B1), it is easy to find that

$$B_j^{-2} = \sum_{l=0}^{\infty} \frac{(1-\eta)^l}{l!} \langle \psi | a^{\dagger l} \eta^n U_{p_j}^\dagger U_{p_j} a^l | \psi \rangle. \quad (\text{B10})$$

To obtain the specific expression of  $B_j^{-2}$ , we employ the technique of integrating within an ordered product of operators [72], i.e.,  $\eta^n n^q =: \partial^q / \partial x^q \{ e^{(\eta e^x - 1)n} \} |_{x=0} :$ , where  $: \cdot :$  indicates the symbol of the normal ordering form, which further leads to the formula

$$\begin{aligned} & \sum_{l=0}^{\infty} \frac{(1-\eta)^l}{l!} l^p a^{\dagger l} \eta^n n^q a^l \\ &= \frac{\partial^{q+p}}{\partial x^q \partial y^p} [\eta e^x + (1-\eta)e^y]^n |_{x=y=0}. \end{aligned} \quad (\text{B11})$$

Then we can obtain the specific forms for  $B_1$  and  $B_2$ , i.e.,

$$B_1 = [1 + (3\eta - \eta^2) \langle \psi | n | \psi \rangle + \eta^2 \langle \psi | n^2 | \psi \rangle]^{-\frac{1}{2}}, \quad (\text{B12})$$

$$B_2 = [(\eta - \eta^2) \langle \psi | n | \psi \rangle + \eta^2 \langle \psi | n^2 | \psi \rangle]^{-\frac{1}{2}}, \quad (\text{B13})$$

where

$$\langle \psi | n | \psi \rangle = \alpha^2 \cosh^2 g + \sinh^2 g, \quad (\text{B14})$$

$$\begin{aligned} \langle \psi | n^2 | \psi \rangle &= \alpha^2 \cosh^2 g + \sinh^2 g + \alpha^4 \cosh^4 g \\ &+ 2 \sinh^4 g + 4\alpha^2 \sinh^2 g \cosh^2 g, \end{aligned} \quad (\text{B15})$$

$$\begin{aligned} \langle \psi | n^3 | \psi \rangle &= \alpha^2 \cosh^2 g + \sinh^2 g + 3\alpha^4 \cosh^4 g \\ &+ 6 \sinh^4 g + 12\alpha^2 \sinh^2 g \cosh^2 g \\ &+ \alpha^6 \cosh^6 g + 18\alpha^2 \cosh^2 g \sinh^4 g \\ &+ 6 \sinh^6 g + 9\alpha^4 \cosh^4 g \sinh^2 g, \end{aligned} \quad (\text{B16})$$

and

$$\begin{aligned} \langle \psi | n^4 | \psi \rangle &= \alpha^2 \cosh^2 g + \sinh^2 g + 7\alpha^4 \cosh^4 g \\ &+ 14 \sinh^4 g + 28\alpha^2 \sinh^2 g \cosh^2 g \\ &+ 36 \sinh^6 g + 6\alpha^6 \cosh^6 g + 24 \sinh^8 g \\ &+ 108\alpha^2 \cosh^2 g \sinh^4 g + \alpha^8 \cosh^8 g \\ &+ 54\alpha^4 \cosh^4 g \sinh^2 g + 96\alpha^2 \cosh^2 g \sinh^6 g \\ &+ 72\alpha^4 \cosh^4 g \sinh^4 g + 16\alpha^6 \cosh^6 g \sinh^2 g. \end{aligned} \quad (\text{B17})$$

Here  $\langle \cdot \rangle$  is the average under the state  $|\psi\rangle$ , and  $|\psi\rangle = U_{S_1} |\alpha\rangle_a |0\rangle_b$  is the state after the first OPA.

Finally, using Eq. (B11) and Eqs. (B2), (B8), and (B9) to derive  $C_{Q_j}$  depending on  $\lambda$  for the PA-then-PS scheme ( $C_{Q_1}$ )

and for the PS-then-PA scheme ( $C_{Q_2}$ ), we have

$$\begin{aligned} C_{Q_1} &= 4 \{ B_1^2 (u_1 \langle \psi | n^4 | \psi \rangle + u_2 \langle \psi | n^3 | \psi \rangle \\ &+ u_3 \langle \psi | n^2 | \psi \rangle + u_4 \langle \psi | n | \psi \rangle) \\ &- [B_1^2 (u_5 \langle \psi | n^3 | \psi \rangle + u_6 \langle \psi | n^2 | \psi \rangle \\ &+ u_7 \langle \psi | n | \psi \rangle)]^2 \} \end{aligned} \quad (\text{B18})$$

and

$$\begin{aligned} C_{Q_2} &= 4 \{ B_2^2 (u_1 \langle \psi | n^4 | \psi \rangle + u_8 \langle \psi | n^3 | \psi \rangle \\ &+ u_9 \langle \psi | n^2 | \psi \rangle + u_{10} \langle \psi | n | \psi \rangle) \\ &- [B_2^2 (u_5 \langle \psi | n^3 | \psi \rangle + u_{11} \langle \psi | n^2 | \psi \rangle \\ &+ u_{12} \langle \psi | n | \psi \rangle)]^2 \}, \end{aligned} \quad (\text{B19})$$

where

$$u_1 = \lambda^2 \eta^4 - 2\lambda^2 \eta^3 + \lambda^2 \eta^2 + 2\lambda \eta^4 - 2\lambda \eta^3 + \eta^4, \quad (\text{B20})$$

$$\begin{aligned} u_2 &= -6\lambda^2 \eta^4 + 14\lambda^2 \eta^3 - 11\lambda^2 \eta^2 + 3\lambda^2 \eta \\ &- 12\lambda \eta^4 + 22\lambda \eta^3 - 10\lambda \eta^2 - 6\eta^4 + 8\eta^3, \end{aligned} \quad (\text{B21})$$

$$\begin{aligned} u_3 &= 11\lambda^2 \eta^4 - 28\lambda^2 \eta^3 + 24\lambda^2 \eta^2 - 8\lambda^2 \eta \\ &+ \lambda^2 + 22\lambda \eta^4 - 52\lambda \eta^3 + 38\lambda \eta^2 \\ &- 8\lambda \eta + 11\eta^4 - 24\eta^3 + 14\eta^2, \end{aligned} \quad (\text{B22})$$

$$\begin{aligned} u_4 &= -6\lambda^2 \eta^4 + 16\lambda^2 \eta^3 - 14\lambda^2 \eta^2 + 4\lambda^2 \eta \\ &- 12\lambda \eta^4 + 32\lambda \eta^3 - 28\lambda \eta^2 + 8\lambda \eta \\ &- 6\eta^4 + 16\eta^3 - 14\eta^2 + 4\eta, \end{aligned} \quad (\text{B23})$$

$$u_5 = \lambda \eta^3 - \lambda \eta^2 + \eta^3, \quad (\text{B24})$$

$$u_6 = 6\lambda \eta^2 - 3\lambda \eta - 3\lambda \eta^3 + 5\eta^2 - 3\eta^3, \quad (\text{B25})$$

$$u_7 = 4\eta - \lambda + 4\lambda \eta - 5\lambda \eta^2 + 2\lambda \eta^3 - 5\eta^2 + 2\eta^3, \quad (\text{B26})$$

$$\begin{aligned} u_8 &= -6\lambda^2 \eta^4 + 12\lambda^2 \eta^3 - 7\lambda^2 \eta^2 + \lambda^2 \eta \\ &- 12\lambda \eta^4 + 18\lambda \eta^3 - 6\lambda \eta^2 - 6\eta^4 + 6\eta^3, \end{aligned} \quad (\text{B27})$$

$$\begin{aligned} u_9 &= 11\lambda^2 \eta^4 - 22\lambda^2 \eta^3 + 13\lambda^2 \eta^2 - 2\lambda^2 \eta \\ &+ 22\lambda \eta^4 - 40\lambda \eta^3 + 20\lambda \eta^2 \\ &- 2\lambda \eta + 11\eta^4 - 18\eta^3 + 7\eta^2, \end{aligned} \quad (\text{B28})$$

$$\begin{aligned} u_{10} &= -6\lambda^2 \eta^4 + 12\lambda^2 \eta^3 - 7\lambda^2 \eta^2 + \lambda^2 \eta \\ &- 12\lambda \eta^4 + 24\lambda \eta^3 - 14\lambda \eta^2 \\ &+ 2\lambda \eta - 6\eta^4 + 12\eta^3 - 7\eta^2 + \eta, \end{aligned} \quad (\text{B29})$$

$$u_{11} = 4\lambda \eta^2 - \lambda \eta - 3\lambda \eta^3 + 3\eta^2 - 3\eta^3, \quad (\text{B30})$$

$$u_{12} = \eta + \lambda \eta - 3\lambda \eta^2 + 2\lambda \eta^3 - 3\eta^2 + 2\eta^3. \quad (\text{B31})$$

Then, we can further optimize  $\lambda$  to get the minimum value of  $C_{Q_j}$  using Eq. (19), which corresponds to  $F_{L_j}$ .

## APPENDIX C: THE WF WITH THE NCO

For a two-mode quantum state  $\rho$ , its WF under the coherence-state representation can be calculated as

$$W_j(z, \gamma) = e^{2(|z|^2 + |\gamma|^2)} \int \frac{d^2\beta_a d^2\beta_b}{\pi^4} \langle -\beta_a, \beta_b | \rho | \beta_a, \beta_b \rangle \times e^{2(z\beta_a^* - z^*\beta_a + \gamma\beta_b^* - \gamma^*\beta_b)}, \quad (\text{C1})$$

where  $j = 1$  or  $2$  and  $|\beta_a, \beta_b\rangle = |\beta_a\rangle \otimes |\beta_b\rangle$  are two-mode coherent states. From Eq. (C1), the analytic expression of the WF can be obtained by providing the density operator  $\rho$  of the quantum state. Here, we consider only the ideal case, i.e., without losses. The quantum state after the NCO is  $|\psi_P\rangle = A_j U_{P_j} U_{S_j} |\alpha\rangle_a |0\rangle_b$ . Therefore, the density operator  $\rho$  can be expressed as

$$\rho = |\psi_P\rangle \langle \psi_P|. \quad (\text{C2})$$

By substituting Eq. (C2) into Eq. (C1), we can obtain the WF after the NCO. Here, the specific expressions are not shown for simplicity.

To clearly observe the effect of the gain factor  $g$  on the nonclassicality of two different non-Gaussian operations ( $aa^\dagger$ ,  $a^\dagger a$ ), we use the negative volume  $V_j$  of the WF to quantitatively describe the nonclassicality of the quantum state after the NCO. The calculation formula for the negative volume  $V_j$  of the WF is given by

$$V_j = \frac{\int dx_1 dx_2 dy_1 dy_2 [|W_j(z, \gamma)| - W_j(z, \gamma)]}{2}, \quad (\text{C3})$$

where  $z = (x_1 + iy_1)/\sqrt{2}$  and  $\gamma = (x_2 + iy_2)/\sqrt{2}$ . According to Eq. (C3), the WF negative volume of state  $|\psi_P\rangle$  can be numerically calculated.

- 
- [1] G. M. D'Ariano and M. G. A. Paris, Arbitrary precision in multipath interferometry, *Phys. Rev. A* **55**, 2267 (1997).
- [2] G. Brida, M. Genovese, and I. R. Berchera, Experimental realization of sub-shot-noise quantum imaging, *Nat. Photon.* **4**, 227 (2010).
- [3] M. A. Taylor, J. Janousek, V. Daria, J. Knittel, B. Hage, H. A. Bachor, and W. P. Bowen, Biological measurement beyond the quantum limit, *Nat. Photon.* **7**, 229 (2013).
- [4] T. Ono, R. Okamoto, and S. Takeuchi, An entanglement-enhanced microscope, *Nat. Commun.* **4**, 2426 (2013).
- [5] R. X. Adhikari, Gravitational radiation detection with laser interferometry, *Rev. Mod. Phys.* **86**, 121 (2014).
- [6] C. Bonato, M. S. Blok, H. T. Dinani, D. W. Berry, M. L. Markham, D. J. Twitchen, and R. Hanson, Optimized quantum sensing with a single electron spin using real-time adaptive measurements, *Nat. Nanotechnol.* **11**, 247 (2016).
- [7] C. Degen, F. Reinhard, and P. Cappellaro, Quantum sensing, *Rev. Mod. Phys.* **89**, 035002 (2017).
- [8] Y. Ma, H. Miao, B. H. Pang, M. Evans, C. Zhao, J. Harms, R. Schnabel, and Y. Chen, Proposal for gravitational-wave detection beyond the standard quantum limit through EPR entanglement, *Nat. Phys.* **13**, 776 (2017).
- [9] S. Pirandola, B. R. Bardhan, T. Gehring, C. Weedbrook, and S. Lloyd, Advances in photonic quantum sensing, *Nat. Photon.* **12**, 724 (2018).
- [10] C. M. Caves, Quantum-mechanical noise in an interferometer, *Phys. Rev. D* **23**, 1693 (1981).
- [11] V. Giovannetti, S. Lloyd, and L. Maccone, Quantum-enhanced measurements: Beating the standard quantum limit, *Science* **306**, 1330 (2004).
- [12] V. Giovannetti, S. Lloyd, and L. Maccone, Advances in quantum metrology, *Nat. Photon.* **5**, 222 (2011).
- [13] A. N. Boto, P. Kok, D. S. Abrams, S. L. Braunstein, C. P. Williams, and J. P. Dowling, Quantum interferometric optical lithography: Exploiting entanglement to beat the diffraction limit, *Phys. Rev. Lett.* **85**, 2733 (2000).
- [14] J. P. Dowling, Quantum optical metrology - the lowdown on high-NOON states, *Contemp. Phys.* **49**, 125 (2008).
- [15] R. A. Campos, C. C. Gerry, and A. Benmoussa, Optical interferometry at the Heisenberg limit with twin Fock states and parity measurements, *Phys. Rev. A* **68**, 023810 (2003).
- [16] P. M. Anisimov, G. M. Raterman, A. Chiruvelli, W. N. Plick, S. D. Huver, H. Lee, and J. P. Dowling, Quantum metrology with two-mode squeezed vacuum: Parity detection beats the Heisenberg limit, *Phys. Rev. Lett.* **104**, 103602 (2010).
- [17] J. Liu, T. Shao, Y. X. Wang, M. M. Zhang, Y. Y. Hu, D. X. Chen, and D. Wei, Enhancement of the phase sensitivity with two-mode squeezed coherent state based on a Mach-Zehnder interferometer, *Opt. Express* **31**, 27735 (2023).
- [18] T. Nagata, R. Okamoto, J. L. O'Brien, K. Sasaki, and S. Takeuchi, Beating the standard quantum limit with four-entangled photons, *Science* **316**, 726 (2007).
- [19] Z. K. Zhao, H. Zhang, Y. B. Huang, and L. Y. Hu, Phase estimation of a Mach-Zehnder interferometer via the Laguerre excitation squeezed state, *Opt. Express* **31**, 17645 (2023).
- [20] M. V. Chekhova and Z. Y. Ou, Nonlinear interferometers in quantum optics, *Adv. Opt. Photon.* **8**, 104 (2016).
- [21] Z. Y. Ou and X. Li, Quantum SU(1,1) interferometers: Basic principles and applications, *APL Photon.* **5**, 080902 (2020).
- [22] B. Yurke, S. L. McCall, and J. R. Klauder, SU(2) and SU(1,1) interferometers, *Phys. Rev. A* **33**, 4033 (1986).
- [23] S. K. Chang, C. P. Wei, H. Zhang, Y. Xia, W. Ye, and L. Y. Hu, Enhanced phase sensitivity with a nonconventional interferometer and nonlinear phase shifter, *Phys. Lett. A* **384**, 126755 (2020).
- [24] S. K. Chang, W. Ye, H. Zhang, L. Y. Hu, J. H. Huang, and S. Q. Liu, Improvement of phase sensitivity in an SU(1, 1) interferometer via a phase shift induced by a Kerr medium, *Phys. Rev. A* **105**, 033704 (2022).
- [25] C. M. Caves, Reframing SU(1,1) interferometry, *Adv. Quantum Technol.* **3**, 1900138 (2020).
- [26] D. Scharwald, T. Meier, and P. R. Sharapova, Phase sensitivity of spatially broadband high-gain SU(1,1) interferometers, *Phys. Rev. Res.* **5**, 043158 (2023).
- [27] F. Hudelist, J. Kong, C. J. Liu, J. T. Jing, Z. Y. Ou, and W. P. Zhang, Quantum metrology with parametric

- amplifier-based photon correlation interferometers, *Nat. Commun.* **5**, 3049 (2014).
- [28] J. Jing, C. Liu, Z. Zhou, Z. Y. Ou, and W. Zhang, Realization of a nonlinear interferometer with parametric amplifiers, *Appl. Phys. Lett.* **99**, 011110 (2011).
- [29] J. Kong, Z. Y. Ou, and W. Zhang, Phase-measurement sensitivity beyond the standard quantum limit in an interferometer consisting of a parametric amplifier and a beam splitter, *Phys. Rev. A* **87**, 023825 (2013).
- [30] B. Chen, C. Qiu, S. Chen, J. Guo, L. Q. Chen, Z. Y. Ou, and W. Zhang, *Phys. Rev. Lett.* **115**, 043602 (2015).
- [31] B. E. Anderson, P. Gupta, B. L. Schmittberger, T. Horrom, C. Hermann-Avigliano, K. M. Jones, and P. D. Lett, Phase sensing beyond the standard quantum limit with a variation on the SU(1,1) interferometer, *Optica* **4**, 752 (2017).
- [32] S. S. Szigeti, R. J. Lewis-Swan, and S. A. Haine, Pumped-up SU(1,1) interferometry, *Phys. Rev. Lett.* **118**, 150401 (2017).
- [33] G. Frascella, E. E. Mikhailov, N. Takanashi, R. V. Zakharov, O. V. Tikhonova, and M. V. Chekhova, Wide-field SU(1,1) interferometer, *Optica* **6**, 1233 (2019).
- [34] J. Liu, Y. Wang, M. Zhang, J. Wang, D. Wei, and H. Gao, Ultra-sensitive phase measurement based on an SU(1,1) interferometer employing external resources and subtract intensity detection, *Opt. Express* **28**, 39443 (2020).
- [35] W. Du, J. F. Chen, Z. Y. Ou, and W. Zhang, Quantum dense metrology by an SU(2)-in-SU(1,1) nested interferometer, *Appl. Phys. Lett.* **117**, 024003 (2020).
- [36] D. Liao, J. Xin, and J. Jing, Nonlinear interferometer based on two-port feedback nondegenerate optical parametric amplification, *Opt. Commun.* **496**, 127137 (2021).
- [37] J. D. Zhang, C. You, C. Li, and S. Wang, Phase sensitivity approaching the quantum Cramér-Rao bound in a modified SU(1,1) interferometer, *Phys. Rev. A* **103**, 032617 (2021).
- [38] H. Ma and Y. Liu, Super-resolution localization microscopy: Toward high throughput, high quality, and low cost, *APL Photon.* **5**, 060902 (2020).
- [39] Y. K. Xu, S. K. Chang, C. J. Liu, L. Y. Hu, and S. Q. Liu, Phase estimation of an SU(1,1) interferometer with a coherent superposition squeezed vacuum in a realistic case, *Opt. Express* **30**, 38178 (2022).
- [40] A. M. Marino, N. V. Corzo Trejo, and P. D. Lett, Effect of losses on the performance of an SU(1,1) interferometer, *Phys. Rev. A* **86**, 023844 (2012).
- [41] Z. Y. Ou, Enhancement of the phase-measurement sensitivity beyond the standard quantum limit by a nonlinear interferometer, *Phys. Rev. A* **85**, 023815 (2012).
- [42] L. Y. Hu, X. X. Xu, Z. S. Wang, X. F. Xu, Photon-subtracted squeezed thermal state: Nonclassicality and decoherence, *Phys. Rev. A* **82**, 043842 (2010).
- [43] L. Hu, M. Al-amri, Z. Liao, and M. S. Zubairy, Entanglement improvement via a quantum scissor in a realistic environment, *Phys. Rev. A* **100**, 052322 (2019).
- [44] L. Hu, Z. Liao, and M. S. Zubairy, Continuous-variable entanglement via multiphoton catalysis, *Phys. Rev. A* **95**, 012310 (2017).
- [45] H. Zhang, W. Ye, Y. Xia, S. K. Chang, C. P. Wei, and L. Y. Hu, Improvement of the entanglement properties for entangled states using a superposition of number-conserving operations, *Laser Phys. Lett.* **16**, 085204 (2019).
- [46] N. Namekata, Y. Takahashi, G. Fujii, D. Fukuda, S. Kurimura, and S. Inoue, Non-Gaussian operation based on photon subtraction using a photon-number-resolving detector at a telecommunications wavelength, *Nat. Photon.* **4**, 655 (2010).
- [47] A. Zavatta, V. Parigi, and M. Bellini, Experimental nonclassicality of single-photon-added thermal light states, *Phys. Rev. A* **75**, 052106 (2007).
- [48] V. Parigi, A. Zavatta, M. Kim, and M. Bellini, Probing quantum commutation rules by addition and subtraction of single photons to/from a light field, *Science* **317**, 1890 (2007).
- [49] W. Ye, H. Zhong, Q. Liao, D. Huang, L. Y. Hu, and Y. Guo, Improvement of self-referenced continuous variable quantum key distribution with quantum photon catalysis, *Opt. Express* **27**, 17186 (2019).
- [50] K. Zhang, Y. Lv, Y. Guo, J. Jing, and W.-M. Liu, Enhancing the precision of a phase measurement through phase-sensitive non-Gaussianity, *Phys. Rev. A* **105**, 042607 (2022).
- [51] A. Zavatta, V. Parigi, M. S. Kim, H. Jeong, and M. Bellini, Experimental demonstration of the Bosonic commutation relation via superpositions of quantum operations on thermal light fields, *Phys. Rev. Lett.* **103**, 140406 (2009).
- [52] H. Zhang, W. Ye, C. P. Wei, C. J. Liu, Z. Y. Liao, and L. Y. Hu, Improving phase estimation using number-conserving operations, *Phys. Rev. A* **103**, 052602 (2021).
- [53] Y. K. Xu, T. Zhao, Q. Q. Kang, C. J. Liu, L. Y. Hu, and S. Q. Liu, Phase sensitivity of an SU(1,1) interferometer in photon-loss via photon operations, *Opt. Express* **31**, 8414 (2023).
- [54] C. W. Helstrom, Minimum mean-squared error of estimates in quantum statistics, *Phys. Lett. A* **25**, 101 (1967).
- [55] C. W. Helstrom, Quantum detection and estimation theory, *J. Stat. Phys.* **1**, 231 (1969).
- [56] A. Zavatta, S. Viciani, and M. Bellini, Quantum-to-classical transition with single-photon-added coherent states of light, *Science* **306**, 660 (2004).
- [57] J. Wenger, R. Tualle-Brouiri, and P. Grangier, Non-Gaussian statistics from individual pulses of squeezed light, *Phys. Rev. Lett.* **92**, 153601 (2004).
- [58] M. Xiao, L. A. Wu, and H. J. Kimble, Precision measurement beyond the shot-noise limit, *Phys. Rev. Lett.* **59**, 278 (1987).
- [59] R. Demkowicz-Dobrzański, M. Jarzyna, and J. Kołodyński, Quantum limits in optical interferometry, *Prog. Optics* **60**, 345 (2015).
- [60] M. Bradshaw, P. K. Lam, and S. M. Assad, Ultimate precision of joint quadrature parameter estimation with a Gaussian probe, *Phys. Rev. A* **97**, 012106 (2018).
- [61] D. Li, C. H. Yuan, Z. Y. Ou, and W. Zhang, The phase sensitivity of an SU(1,1) interferometer with coherent and squeezed-vacuum light, *New J. Phys.* **16**, 073020 (2014).
- [62] X. Y. Hu, C. P. Wei, Y. F. Yu, and Z. M. Zhang, Enhanced phase sensitivity of an SU(1,1) interferometer with displaced squeezed vacuum light, *Front. Phys.* **11**, 114203 (2016).
- [63] D. Li, B. T. Gard, Y. Gao, C. H. Yuan, W. Zhang, H. Lee, and J. P. Dowling, Phase sensitivity at the Heisenberg limit in an SU(1,1) interferometer via parity detection, *Phys. Rev. A* **94**, 063840 (2016).
- [64] S. Ataman, A. Preda, and R. Ionicioiu, Phase sensitivity of a Mach-Zehnder interferometer with single-intensity and difference-intensity detection, *Phys. Rev. A* **98**, 043856 (2018).

- [65] D. Li, C. H. Yuan, Y. Yao, W. Jiang, M. Li, and W. Zhang, Effects of loss on the phase sensitivity with parity detection in an SU(1,1) interferometer, *J. Opt. Soc. Am. B* **35**, 1080 (2018).
- [66] L. Hu, M. Al-amri, Z. Liao, and M. S. Zubairy, Continuous-variable quantum key distribution with non-Gaussian operations, *Phys. Rev. A* **102**, 012608 (2020).
- [67] Y. Guo, W. Ye, H. Zhong, and Q. Liao, Continuous-variable quantum key distribution with non-Gaussian quantum catalysis, *Phys. Rev. A* **99**, 032327 (2019).
- [68] J. Beltran and A. Luis, Breaking the Heisenberg limit with inefficient detectors, *Phys. Rev. A* **72**, 045801 (2005).
- [69] B. M. Escher, R. L. de Matos Filho, and L. Davidovich, General framework for estimating the ultimate precision limit in noisy quantum-enhanced metrology, *Nat. Phys.* **7**, 406 (2011).
- [70] C. W. Helstrom, *Quantum Detection and Estimation Theory* (Academic Press, New York, 1976), p. 123.
- [71] R. Filip, Gaussian quantum adaptation of non-Gaussian states for a lossy channel, *Phys. Rev. A* **87**, 042308 (2013).
- [72] H. Y. Fan, H. L. Lu, and Y. Fan, Newton-Leibniz integration for ket-bra operators in quantum mechanics and derivation of entangled state representations, *Ann. Phys. (NY)* **321**, 480 (2006).